Water-in-CO2 microemulsions stabilized by an efficient catanionic surfactant

Water-in-CO_2 microemulsions stabilized by an efficient catanionic surfactant

Journal:	*Langmuir*
Manuscript ID	la-2020-00970b.R3
Manuscript Type:	Article
Date Submitted by the Author:	12-Jun-2020
Complete List of Authors:	Sagisaka, Masanobu; Hirosaki University , Graduate School of Science and Technology Saito, Tatsuya; Hirosaki University , Graduate School of Science and Technology Abe, Masashi; Hirosaki University , Graduate School of Science and Technology Yoshizawa, Atsushi; Hirosaki University , Department of Frontier Materials Chemistry Blesic, Marijana; Queen's University Belfast, School of Chemistry and Chemical Engineering Rogers, Sarah; ISIS-STFC Neutron Scattering Facility, Harwell Science and Innovation Campus Alexander, Shirin; Swansea University, College of Engineering Guittard, Frédéric; Universite Cote d'Azur Hill, Christopher; University of Bristol, School of Chemistry Eastoe, Julian; University of Bristol, School of Chemistry

Water-in-CO_2 microemulsions stabilized by an efficient catanionic surfactant

Masanobu Sagisaka[1], Tatsuya Saito[1], Masashi Abe[1], Atsushi Yoshizawa[1], Marijana Blesic[2], Sarah E. Rogers[3], Shirin Alexander[4], Frédéric Guittard[5], Christopher Hill[6], Julian Eastoe[6]*

[1] Department of Frontier Materials Chemistry, Graduate School of Science and Technology, Hirosaki University, 3 Bunkyo-cho, Hirosaki, Aomori 036-8561, JAPAN

[2] School of Chemistry and Chemical Engineering, Queen's University Belfast, University Road, Belfast, BT7 1NN, U.K.

[3] ISIS-CCLRC, Rutherford Appleton Laboratory, Chilton, Oxon OX11 0QX, U.K.

[4] Energy Safety Research Institute (ESRI), Swansea University, Bay Campus, Swansea SA1 8EN, UK.

[5] Univ. Cote d'Azur, NICE-Lab, 61-63 av. S. Viel, 06200 Nice, France

[6] School of Chemistry, University of Bristol, Cantock's Close, Bristol BS8 1TS, U.K.

*To whom all correspondence should be addressed

Masanobu SAGISAKA E-mail: sagisaka@hirosaki-u.ac.jp Phone and Fax: +81-172-39-3579

Abstract

To facilitate potential applications of water-in-supercritical CO_2 microemulsions (W/CO_2 μEs) efficient and environmentally responsible surfactants are required with low levels fluorination. As well as being able to stabilize water-CO_2 interfaces, these surfactants must also be economical, prevent bio-accumulation and strong adhesion, deactivation of enzymes, and also be tolerant to high salt environments. Recently, an ion paired catanionic surfactant with environmentally-acceptable fluorinated C_6-tails was found to be very effective at stabilizing W/CO_2 μEs with high water-to-surfactant molar ratios (W_0) up to ~50 (Sagisaka, M. et al. *Langmuir*, **2019**, *35*, 3445–3454). As the cationic and anionic constituent surfactants alone did not stabilize W/CO_2 μEs, this was the first demonstration of surfactant synergistic effects in W/CO_2 microemulsions. The aim of this new study is to understand the origin of these intriguing effects by detailed investigations of nanostructure in W/CO_2 microemulsions using high pressure small-angle neutron scattering (HP-SANS). These HP-SANS experiments have been used to determine the headgroup interfacial area and volume, aggregation number and effective packing parameter (EPP). These SANS data suggest the effectiveness of this surfactant originates from increased EPP and decreased hydrophilic/CO_2-philic balance, related to a reduced effective headgroup ionicity. This surfactant bears separate C_6F_{13}-tails and oppositely-charged headgroups, and was found to have a EPP value similar to that of a double C_4F_9-tail anionic surfactant (4FG(EO)$_2$), which was previously reported to be one of most efficient stabilizers for W/CO_2 μEs (maximum W_0 = 60-80). Catanionic surfactants based on this new design will be key for generating super-efficient W/CO_2 μEs with high stability and water solubilization.

Keywords: Supercritical CO_2, Microemulsion, Catanionic Surfactant, Solubilizing Power, Small-Angle Neutron Scattering

Introduction

Supercritical CO_2 ($scCO_2$) is now widely used industrially as an alternative solvent to replace volatile organic compounds (VOCs) for organic synthesis, dry cleaning, polymerization, extraction, and nanomaterial processing amongst others[1]. For these applications there are numerous advantages of $scCO_2$ such as low cost, non-toxicity, non-flammability, natural abundance, a solvent quality tunable by control over pressure and temperature, and elimination of energy-consuming solvent evaporation steps in separation processes[1]. One of the drawbacks of pure $scCO_2$ for applications is the inherent low solubility of polar solutes: approaches to overcome this are required to help develop further industrial applications of $scCO_2$. An obvious way to enhance low solubility is though formation of water-in-$scCO_2$ (W/CO_2) dispersions, including microemulsions (μEs) and macroemulsions (emulsions): numerous surfactants have been tested to accomplish this task[2-13]. However, conventional hydrocarbon (HC) surfactants typically used for analogous water-oil μEs, including Aerosol-OT (sodium bis-(2-ethyl-1-hexyl) sulfosuccinate, AOT)[14], are essentially incompatible with pure $scCO_2$ [3-7]. On the other hand, some specialized tailor-made fluorocarbon (FC) surfactants have been found to display high affinity for $scCO_2$, and are able to stabilize W/CO_2 μEs with modest water-to-surfactant molar ratios > 10 (W_0 = [water]/[surf]).[7-13] These CO_2-philic FC surfactants may consist of either perfluoropolyether (PFPE)-tails, double FC-tail and FC-HC hybrid-tail structures.[7-13] For example, a single PFPE-tail surfactant ($PFPECOONH_4$), a hybrid surfactant having perfluorohexyl and *n*-butyl tails (FC6-HC4), and double perfluorocarbon-tail surfactants ($8FS(EO)_2$, $8FG(EO)_2$ and $4FG(EO)_2$) (**Figure S1** for chemical structures) have been shown to stabilize W/CO_2 μEs with maximum W_0 (W_0^{max}) values up to 20, 80 and 45-80, respectively.[7-13] These surfactants mentioned are mainly anionic which presents problems for applications, including, difficulties of removing ionic surfactants from processes producing nanoparticles, deactivation with enzymatic reactions, surfactant-dye complexation in dyeing, and salting-out at high salinities typical in enhanced oil recovery (EOR)[15-19]. For industrial applications CO_2-philic surfactants should ideally be composed of (1) CO_2-philic tails with low fluorination for reducing cost and environmental impact, and (2) possess nonionic or weakly ionic headgroups to minimize salting out.

Earlier studies [20,21] investigated synergistic effects on interfacial properties of $scCO_2$-philic surfactants by mixing HC, FC and FC-HC surfactants (**Figure S1**). Mixing commercial nonionic HC surfactants (TMN-6 and L31, **Figure S1**) with fluorinated surfactants reduced the critical microemulsion concentration (*cμc*), which is defined as the lowest surfactant concentration to yield a microemulsion, compared to the individual surfactants, however, synergistic effects were not observed in terms of the water-solubilization W_0 [20]. On the other hand, mixing $8FS(EO)_2$ and FC6-HC4 (**Figure S1**) increased W_0^{max} by only 3 compared with the value for each surfactant at 75 ºC and 400 bar, showing a very small synergistic effect [21].

In earlier studies of surfactant mixtures in conventional solvents, the combination of anionic and cationic surfactants was shown to result in strong synergism in terms of interfacial properties, stability of vesicles, reverse-type molecular assemblies and W/O dispersions [22,23]. In these cases, synergism is understood to originate from electrostatic interactions between oppositely charged headgroups. These cationic:anionic surfactant mixtures have been simplified further still, by synthesizing pure catanionic surfactants excluding the counterions.[24]

A previous study reported synthesis of three pure catanionic surfactants ($[C_6F_{13}mim][(CF_3)_3S]$, $[C_6F_{13}mim][C_6F_{13}S]$ and $[C_5F_{11}mim][C_5F_{11}S]$, **Figure 1**) bearing environmentally-acceptable short chain FC tails, and studied formation and properties of W/CO_2 μEs.[25] One of the these surfactants, namely $[C_6F_{13}mim][C_6F_{13}S]$, showed exceptional water-solubilizing power (W_0^{max} = ~50) , representing the first observation of surfactant synergism in W/CO_2 μEs. The catanionic surfactants were shown to display cloud point temperatures, rather than Kraft temperatures, suggesting the catanionic headgroup has some nonionic character[25].

To clarify the mechanism of synergism and ion pairing with these CO_2-active catanionic surfactants this study investigates phase behavior, solubilizing properties and self-assembly structure of W/CO_2 μEs at different pressures and W_0 values. Probe dye studies, using UV-vis absorption spectra with an ionic dye methyl orange was used to follow water uptake and high-pressure small-angle neutron scattering (HP-SANS) was used to determine microemulsion water droplet structures and sizes. The

SANS measurements have permitted an assessment of the effective packing parameter (EPP, in other words, an intrinsic packing parameter relevant to an individual mixed system under certain experimental conditions)[26-29] to be made. The EPP is a key index, indicating the preferred self-assembly structure, and is based on surfactant spatial packing, resulting from interactions with solvents (water and CO_2) and neighboring surfactant molecules. These results demonstrate that catanionic surfactants can offer new insight into the design criteria for inexpensive and environmental-friendly surfactants for W/CO_2 μEs appropriate for industrial use.

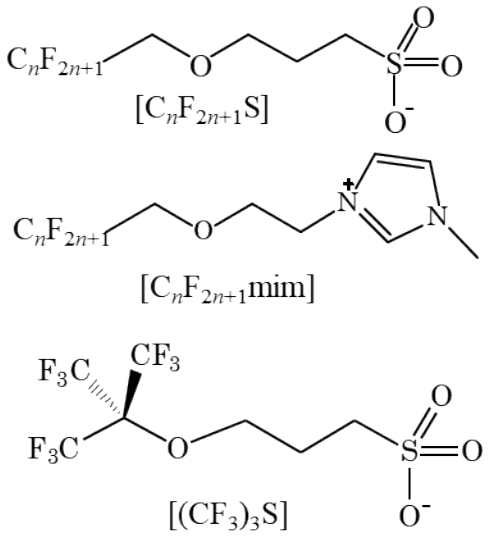

Figure 1 Chemical structures of surfactant ions (n =5 or 6).

Experimental Section

Materials

The catanionic surfactants $[C_6F_{13}mim][(CF_3)_3S]$, $[C_6F_{13}mim][C_6F_{13}S]$ and $[C_5F_{11}mim][C_5F_{11}S]$ (**Figure 1**, purity > 95 %) used here were synthesized and purified as described in a previous study[25]. Ultrapure water with a resistivity of 18.2 MΩ cm was obtained from a Millipore Milli-Q Plus system. CO_2 was of 99.99% purity (Ekika Carbon Dioxide Co., Ltd.). Methyl orange was purchased from Acros organics and used without further purification.

Phase behavior observations and UV-visible absorption spectroscopy

A high-pressure (HP) cell with a metal-to-glass sealed glass window (KP-308-3, Nihon Klingage co., ltd) and a moveable piston inside the cell was employed to examine the phase behaviour of surfactant/water/scCO_2 mixtures by operating pressure and temperature. A detailed description of the experimental apparatus and procedures is given in earlier papers.[12,13,25]

Uptake of water into W/CO_2 μEs was examined by UV-visible absorption spectroscopy measurements in a pressure cell (stainless steel SUS316: cell volume 1.5 cm^3) with three quartz windows (thickness: 8 mm, inner diameter: 10 mm). The spectral measurements were performed with a double-beam spectrophotometer (Hitachi High-Technologies, Co., U-2810). Each window was positioned to provide a perpendicular 10-mm optical path. The windows were attached and fastened tightly to the stainless steel body of the cell with PTFE kel-F packing, thereby compressing the packing between the stainless steel parts and the windows, providing excellent sealing (tested up to 400 bar); temperature was controlled by circulating water thermostat bath.

The spectroscopic measurements of the water/surfactant/scCO_2 systems were performed at 350 bar and 45 or 75 °C. The densities of CO_2 were calculated using the Span-Wagner equation of state (EOS) [30]. Pre-determined amounts of surfactant and CO_2, where the molar ratio of surfactant to CO_2 was fixed at 8×10^{-4}, were loaded into the optical cell. An aqueous solution containing methyl orange (MO) as a

trace marker dye (3 mM) was then added into the optical cell through a six-port valve until the clear single-phase Winsor-IV W/CO_2 μE microemulsion converted into a turbid emulsion or hydrated surfactant was seen to precipitate. During spectroscopic measurements, the scCO_2 mixtures were stirred by a magnetic stirrer.

High-Pressure small-angle neutron scattering (SANS) measurements and data analyses

Due to the range of neutron wavelengths available, time-of-flight (T-O-F) SANS is suitable for studying the shapes and sizes of colloidal systems. High-pressure SANS (HP-SANS) is a particularly important technique for determining aggregated nanostructures in supercritical CO_2 [10,12,13,25]. The HP-SANS measurements were performed at 45 °C at various pressures using the SANS2D T-O-F instrument, at the Rutherford Appleton Laboratory at ISIS UK, in conjunction with a stirred, high-pressure cell (Thar). The cell path length and the incident neutron beam diameter were both 10 mm. The measurements gave absolute scattering cross sections $I(Q)$ (cm^{-1}) as a function of momentum transfer Q ($Å^{-1}$), which is defined as $Q = (4\pi/\lambda)\sin(\theta/2)$, where θ is the scattering angle. The accessible Q range was 0.002-1.0 $Å^{-1}$ on SANS2D arising from a white neutron beam with incident wavelengths, λ, of 2.2-10 Å. The data were normalized for transmission, empty cell, solvent background, and pressure induced changes in cell volume as before[12,13,25].

Pre-determined amounts of D_2O and surfactant, where the molar ratio of surfactant to CO_2 was fixed at 8.0×10^{-4} (= 16.7 mM at the appropriate experimental condition), were loaded into the Thar cell. Then CO_2 (11.3 g) was introduced into the cell by using a high-pressure pump, and the surfactant/D_2O/CO_2 mixture was pressurized to 120, 200 or 350 bar at 45 ºC by decreasing the inner volume of the cell. Under vigorous stirring, visual observations were carried out to identify the mixture as being a transparent single-phase (W/CO_2 μE) or a turbid phase. Finally, the HP-SANS experiments were performed for not only single-phase W/CO_2μEs, but also turbid phases formed below the cloud point phase transition pressure P_{trans}. Due to the systems being dilute dispersions (volume fractions typically ≤

0.012), the physical properties of the continuous phase of $scCO_2$ were assumed to be equivalent to those of pure CO_2. The scattering length density (SLD) of reversed micelle shells (ρ_{shell}) was calculated as $\rho_{shell} = 2.28 \times 10^{10}$ cm^{-2}. The SLDs of CO_2 (ρ_{CO2}) and aqueous cores (ρ_{core}) containing the catanionic headgroup in the D_2O/CO_2 μE are variables of CO_2 density and W_0, and are estimated as; $\rho_{CO2} / (10^{10}\,\text{cm}^{-2}) = 2.29$ at 350 bar, 2.03 at 200 bar, and 1.64 at 120 bar, and $\rho_{core} / (10^{10}\,\text{cm}^{-2}) = 3.34$ at $W_0 = 5$, 4.15 at $W_0 = 10$, 4.62 at $W_0 = 15$, 4.92 at $W_0 = 20$, 5.13 at $W_0 = 25$, 5.28 at $W_0 = 30$ and 5.40 at $W_0 = 35$ as estimated in supporting information (see **S2)**. As ρ_{shell} was close to ρ_{CO2} and the shells are solvated with CO_2, neutron scattering from the shells was assumed to be negligible owing to the small contrast step. Therefore, SANS from the D_2O/CO_2 μEs was assumed to only be from the so-called aqueous core contrast. For model fitting data analysis, the W/CO_2 μE droplets were treated as ellipsoidal particles with a Schultz distribution in core radii [31]. The polydispersities in ellipsoid radii were fixed at 0.3 as found in spherical D_2O/CO_2 μEs with the double FC-tail surfactants (polydispersity = 0.17-0.40) [12,13,25]. Full accounts of the scattering laws are given elsewhere [12,13,25,32]. Data have been fitted to the models described above using the SasView small-angle scattering analysis software package (http://www.sasview.org/)[12,13,25,32]. The fitted parameters are the core radii perpendicular to the rotation axis ($R_{f\text{-}ell,a}$) and along the rotation axis ($R_{f\text{-}ell,b}$) for ellipsoidal particles; prior to full model fitting micellar dimensions were initially estimated by Guinier analysis ($R_{g\text{-}sph}$) [33]. The catanionic reverse micelles have C_6-perfluorocarbon tails shells, which weakly interact with other,[25]. The hard sphere model was employed as an effective S(Q) for all W_0 values.

Results and Discussion

Aggregation behavior of catanionic surfactant reverse micelles in water/supercritical CO_2 mixtures

In a previous study, visual observation and FT-IR spectra measurements for 16.7 mM $[C_6F_{13}mim][C_6F_{13}S]$/W/$CO_2$ μEs were conducted.[25] Those results showed formation of transparent single-phases W/CO_2 μE at pressures above P_{trans} in **Fig. S2**, and absorbance characteristic of hydrogen bonded water increased with loading water over the W_0 range from 0 to 50 at 45 ºC and 350 bar, suggesting a high water-solubilizing power of $W_0^{max} = 50$.[25] Here, to confirm this observation, solubilization of water and the tracer ionic dye (aqueous methyl orange MO 3 mM) by $[C_6F_{13}mim][C_6F_{13}S]$ reverse micelles was examined. The dye solution was loaded into 16.7 mM catanionic surfactant/CO_2 mixtures, and the UV-vis adsorption spectra were measured at different W_0 values. Alone, MO does not dissolve in pure CO_2 but it does dissolve in water, and is generally incorporated within the water-rich pockets of single-phase W/CO_2 μEs, dyeing the systems red.[12,13] The surfactant $[C_6F_{13}mim][C_6F_{13}S]$ formed transparent and reddish single–phase CO_2 systems with the MO solution, however, the other catanionic surfactants always remained as precipitates, yielding undyed CO_2 phases.

The UV-vis spectra of MO for $[C_6F_{13}mim][C_6F_{13}S]$ and the other catanionic surfactants are displayed in **Figures 2** and **S3** (supporting information), respectively. At 45 ºC the spectra showed large and broad absorption peaks of MO, and an absorbance maximum (λ_{max}) at ~418 nm independent of W_0. As λ_{max} is known to shift to longer wavelengths[12,13] when MO molecules are solubilized in more polar environments, hence λ_{max} can be employed to gauge microenvironment polarity. Previous experiments with W/CO_2 μEs with anionic hybrid surfactants FC6-HC*n* and double FC-tail surfactants *n*FG(EO)$_2$ and *n*FS(EO)$_2$ displayed λ_{max} values at ~420 nm even at different W_0 values and temperatures of 45 and 75 ºC,[12,13] consistent with free MO molecules solubilized in the aqueous cores. The similar λ_{max} values for anionic and catanionic surfactants imply that the microenvironmental polarity surrounding MO molecules was essentially unaffected by the different kinds of headgroups, most likely as a result of weak interactions between headgroups and MO molecules.

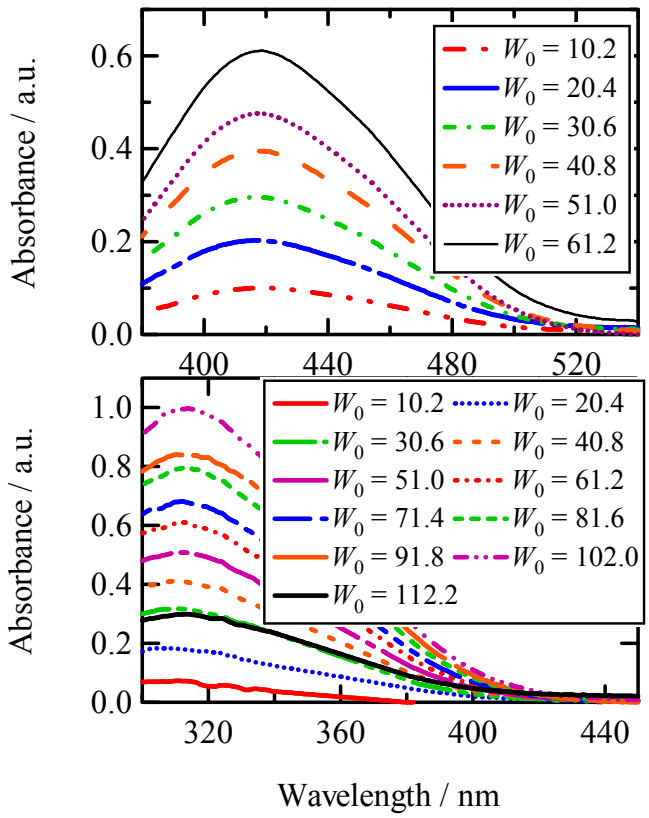

Figure 2 UV-vis spectra of 16.7mM $[C_6F_{13}mim][C_6F_{13}S]$/water/$CO_2$ mixtures with different W_0 values at 350 bar and 45 ºC (Top) or 75 ºC (bottom). 3 mM methyl orange aqueous solution was loaded as a dispersed aqueous phase.

Interestingly, the λ_{max} values blue-shifted to ~314 nm elevating temperature from 45 ºC to 75 ºC, suggesting a notable change in microenvironment. Such blue shifts with MO have been reported in studies in MO/catanionic surfactant/water mixtures, explained by generation of ion pair complexes of MO and cationic surfactants.[34] This suggests that at the high temperature cation-anion dissociation of the catanionic surfactant promoted and then formed anionic MO-cationic $[C_6F_{13}mim]$ ion pair complexes.

As shown in **Figure 2**, the adsorption peaks grew on increasing the dosing of MO solution and the systems remained transparent. To determine the maximum water solubilization (W_0^{max}) of the surfactant at each temperature, the maximum absorbance was plotted as a function of W_0 as shown in **Figure S4**.

The linear behavior seen over the W_0 ranges of 0-61.2 at 45 ºC and of 0-102 at 75 ºC is consistent with W_0^{max} values to be ~60 and ~100, respectively. The W_0^{max} value at 45 ºC was in line with results from FT-IR spectroscopy in a previous study (W_0^{max} = ~50)[25]. Such a high value for W_0^{max} over 50 is quite rare and can be identified with a highly efficient surfactant for stabilizing W/CO_2 microemulsions. On the other hand, no MO absorption was observed for the catanionic surfactants [C_6F_{13}mim][$(CF_3)_3$S] and [C_5F_{11}mim][C_5F_{11}S] (**Figure S3**), suggesting that droplet W/CO_2 μEs, do not form. Since the constituent surfactants of these catanionic surfactants are insoluble and unable to stabilize W/CO_2 μEs,[25] the synergistic effect of pairing of surfactant anions and cations has been clearly demonstrated by the formation of [C_6F_{13}mim][C_6F_{13}S]/W/CO_2 microemulsions, which have notably enhanced stability at 75 ºC.

An important question remaining from the previous study [25] is "why does only [C_6F_{13}mim][C_6F_{13}S] stabilize W/CO_2 μEs, whereas the other surfactants do not?". The structural differences between [C_6F_{13}mim][$(CF_3)_3$S], [C_6F_{13}mim][C_6F_{13}S] and [C_5F_{11}mim][C_5F_{11}S] are small, with just two more CF_2 units for [C_6F_{13}mim][C_6F_{13}S] than the others. Based on previous studies[7,12,13,32] the longer double FC-tails in [C_6F_{13}mim][C_6F_{13}S] would be expected to lead to higher CO_2-philicity and a greater solubility in scCO_2. It seems that the total fluorination is important, and for this class of surfactants there is a critical number of 12 fluorinated carbons needed for stabilization of microemulsions. In other words, surfactants must (1) be sufficiently compatible (soluble) in scCO_2 to adsorb strongly at the water-CO_2 interface and (2) have sufficiently thick FC-shells to maintain droplet stability. These phase behavior studies indicate that [C_6F_{13}mim][C_6F_{13}S] is an optimized surfactant for stabilizing W/CO_2 μEs with high water loadings over W_0^{max} > 50. Furthermore, despite the different catanionic structure, this twin-tailed surfactant is comparable to other super-efficient CO_2-philic surfactants 8FG(EO)$_2$ and FC6-HC4 which instead bear two tails covalently bound to the anionic headgroup [7,12,13,32].

Nano-structure of the catanionic surfactant/W/CO_2 microemulsions

A previous study of $[C_6F_{13}mim][C_6F_{13}S]$/W/$CO_2$ μEs with W_0 = 10 at 350 bar and 45 ºC [25], the SANS profiles were showed the HP-SANS profiles to be consistent with an ellipsoidal form factor model. To clarify changes in the core nanostructure with W_0 and pressure, SANS $I(Q)$ profiles were measured at 45 ºC, W_0 = 5-35 and P = 120-350 bar. SANS data along with the fitted $I(Q)$ functions are shown in **Figure 3** (or **Figure S5**). The SANS profiles of $[C_6F_{13}mim][C_6F_{13}S]$/$D_2O$/$CO_2$ mixtures with $W_0 \leq$ 20-25 at 200-350 bar and ≤ 10 at 120 bar show a gradient of ~0 for the log $[I(Q)]$−log Q plot at $Q < 0.03$ Å^{-1}, suggesting formation of globular nanosized D_2O cores. All SANS data were always measured under stirring. On the other hand, when W_0 was ≥ 25 at 200-350 bar the scattering intensity increased with decreasing Q at $Q <$ 0.02 Å^{-1}, displaying gradients of ~Q^{-4}. At high W_0 values ≥ 25 separated water probably remained in the systems, and was dispersed as equilibrium W/CO_2 emulsion droplets owing to the stirring W/CO_2 μEs. The SANS also showed gradients of ~Q^{-4} at $Q < 0.02$ Å^{-1}.

As a first step in SANS data analysis, Guinier [33] and Porod [35] plots were used to estimate the D_2O core radii (**Figures S6 and S7**), and the results are listed in **Table S1**. The Porod plot asymptote at high Q can be used to analyze interfacial area per surfactant molecule [35]. Unfortunately, reliable asymptotic $\{I(Q)\,Q^4\}_{Q\to\infty}$ values could not be obtained due to a combination of weak scattering and background noise as shown in **Figure S7**. SANS data were also analyzed with Ornstein-Zernicke formalism to investigate density fluctuations in a system approaching critical demixing or phase separation.[36-38] The correlation lengths ξ, showing sizes characteristic of such structural domains are plotted as a function of W_0 in **Figure S9**. The ξ values were found to increase from ~12 Å to ~30 Å with increasing W_0 from 10 to 35 and the increasing trends of ξ were similar to those radii obtained from Porod ($R_{p\text{-}sph}$) and form fitting analysis (**Figure 4**). The $\boldsymbol{R_{g\text{-}sph}}$ values from Guinier analysis were employed as initial radii in the subsequent fitting using models for polydisperse Schultz spherical or ellipsoidal particles, as appropriate for giving the best fits. In the case of ellipsoids, both oblate and prolate aspect ratios were compared (**Figure S5**), and the prolate model gave better fits.

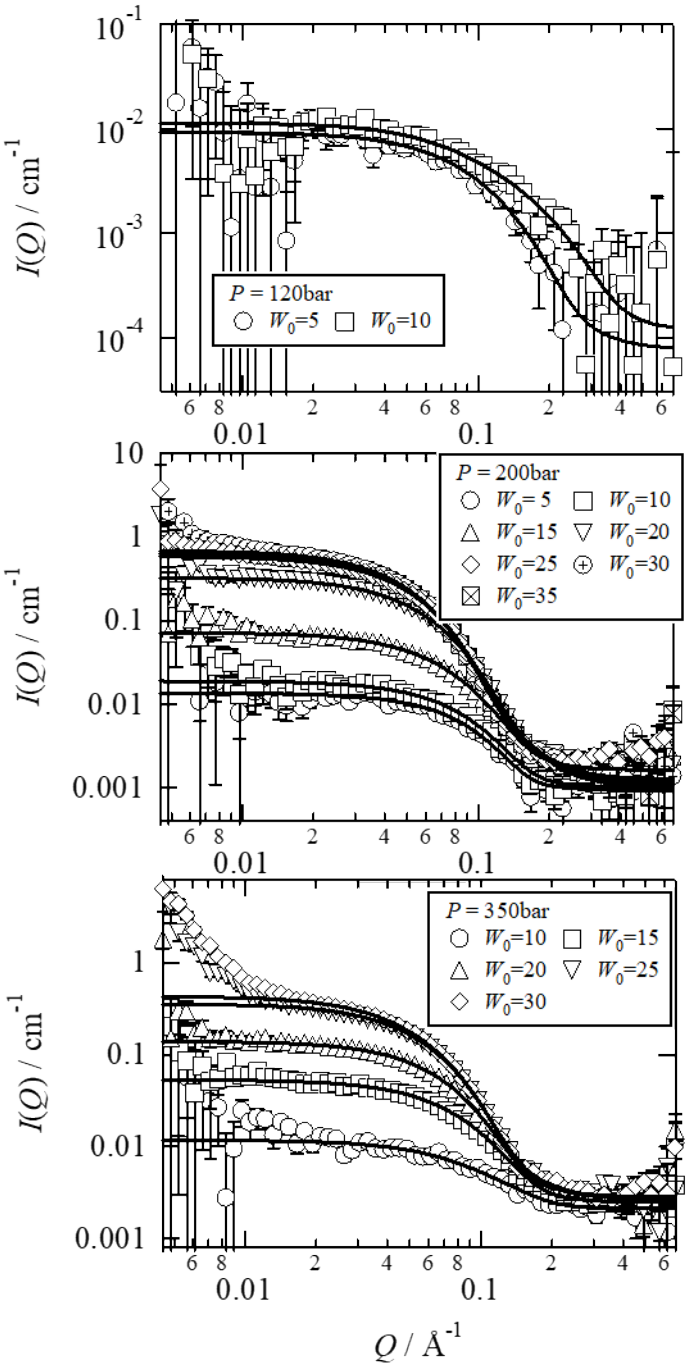

Figure 3. SANS profiles of D_2O/CO_2 μE with 16.7 mM $[C_6F_{13}mim][C_6F_{13}S]$ with different W_0 values at 45 ºC and 120-350 bar. Solid lines are theoretical curves of prolate ellipsoid particle model fitted to the experimental data.

The model fit parameters for the prolate D_2O core μE droplets ($R_{f\text{-}ell,a}$ and $R_{f\text{-}ell,b}$) are listed in **Table S3**. To demonstrate droplet growth with increased loading water, equatorial ($R_{ell\text{-}a}$) and polar ($R_{ell\text{-}b}$) radii of prolate D_2O cores are plotted in **Figure 4** as a function of W_0 at pressures ≥ 200 bar.

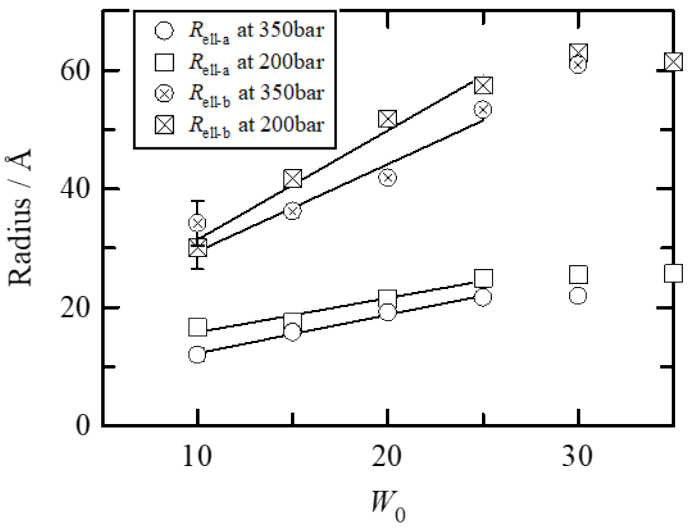

Figure 4. Change in prolate ellipsoid radii ($R_{ell\text{-}a}$ and $R_{ell\text{-}b}$) for 16.7 mM $[C_6F_{13}mim][C_6F_{13}S]/D_2O/CO_2$ μE cores as a function of W_0 at 45 ºC and 200 bar or 350 bar.

As seen in **Table S3** at 120 bar the radii reduced with increasing W_0 from 5 to 10, which was accompanied by a phase transition from transparent μEs to turbid phases (i.e. Winsor IV → stirred Winsor II W/CO_2 microemulsions). On the other hand, at pressures ≥ 200bar, the oblate radii increased linearly with W_0 as up to $W_0 = 25$, being described by $(R_{ell\text{-}a} / Å) = \boldsymbol{a}_{ell\text{-}a} + \boldsymbol{b}_{ell\text{-}a} W_0$ and $(R_{ell\text{-}b} / Å) = \boldsymbol{a}_{ell\text{-}b} + \boldsymbol{b}_{ell\text{-}b} W_0$ (where $\boldsymbol{a}_{ell\text{-}a}$, $\boldsymbol{b}_{ell\text{-}a}$, $\boldsymbol{a}_{ell\text{-}b}$, $\boldsymbol{b}_{ell\text{-}b}$ = 10.0, 0.58, 13.0, 1.84 at 200 bar, and 5.79, 0.65, 14.7, 1.47 at 350 bar. Eventually, the radii reached $R_{ell\text{-}a}$ = ~26 Å and $R_{ell\text{-}b}$ = ~63 Å at 200 bar, and $R_{ell\text{-}a}$ = ~22 Å and $R_{ell\text{-}b}$ = ~61 Å at 350 bar. This is consistent with swelling behavior with loading water as commonly reported in W/O and W/CO_2 reverse microemulsions [13,32,39] . The radii values seemed to plateau for $W_0 > 30$ and visually these systems were turbid, consistent with stirred separating Winsor II phases. The slight discrepancies with W_0^{max} obtained by spectroscopically may be due to weak stirring power in the pressure

cell and/or use of D_2O instead of H_2O needed for the HP-SANS experiments. In contrast with the increasing trend of radii with W_0, the aspect ratios ($R_{ell\text{-}b}$ / $R_{ell\text{-}a}$) were very similar (1.8-2.9) and seemed to be independent of pressure and W_0 as shown in **Figure S10**. The formation of elongated reverse micelles is an interesting observation, and is expected to increase CO_2 viscosity, which may find applications in CO_2-EOR efficiency [13,40,41]. Using equations (S4) and (S5) in supporting information (Sec **S9**), apparent intrinsic and specific viscosities, [η] and η_{sp}, were estimated (**Table S3**). The viscosity enhancements predicted this way would only be modest, ~13 % or less compared with that of pure CO_2. Hence, higher surfactant concentration could be needed to promote higher CO_2 thickening.

Previous SANS studies of double FC-tail surfactants nFG(EO)$_2$ with different FC lengths (n = 4-8) also found a linear relationship between spherical D_2O core radius, R_c, and W_0 where $R_c = \boldsymbol{a} + \boldsymbol{b}\ W_0$, and the constants $\boldsymbol{a}$ = 5.0-5.4 and $\boldsymbol{b}$ = 0.60-0.64 [32]. The average values $\boldsymbol{a}$ and $\boldsymbol{b}$ of prolate core radii for $[C_6F_{13}mim][C_6F_{13}S]/D_2O/CO_2$ microemulsions, namely $\boldsymbol{a} = (2\boldsymbol{a}_{ell\text{-}a}+\boldsymbol{a}_{ell\text{-}b})/3$ and $\boldsymbol{b} = (2\boldsymbol{b}_{ell\text{-}a}+\boldsymbol{b}_{ell\text{-}b})/3$, were 11.0 and 1.00 at 200 bar and 8.8 and 0.92 at 350 bar, and these are 1.7-2.1 and 1.5-1.6 times larger than those for nFG(EO)$_2$, respectively. For spherical geometry the volume of surfactant headgroup (v_{head}) and area per surfactant molecule (A), respectively are related by equation (1)

$$\alpha(p)\ R_c = (3v_{head}/A) + (3v_w/A)\ W_0 \quad (1)$$

where $\alpha(p) = 1 + 2p^2$, p is polydispersity index (σ/R_c), R_c is the core radius, and v_w is volume of a water molecule [13,32]. It follows that the larger $\boldsymbol{a}$ and $\boldsymbol{b}$ values suggests $[C_6F_{13}mim][C_6F_{13}S]$ to have a larger v_{head} and a smaller A than for the nFG(EO)$_2$ series. Based on Equation (1), a volume-to-surface area ratio per aqueous core in reverse μE (v_{core}/s_{core}) can be expressed as,

$$\alpha(p)\ (v_{core}/s_{core}) = (v_{head}\ N_{agg} + v_w\ W_0\ N_{agg}) / (A\ N_{agg}) = (v_{head}/A) + (v_w/A)\ W_0 \quad (2)$$

where N_{agg} is aggregation number. [13,32] An advantage of using Equation (2) is that it can be applied to a wide range of morphologies (spheres, ellipsoids, rods etc), whereas Equation (1) relates only to spherical morphology. Using equation 2 and assuming constant v_{head} and A for $[C_6F_{13}mim][C_6F_{13}S]$, ($v_{core}/s_{core}$) values calculated from $R_{ell\text{-}a}$ and $R_{ell\text{-}b}$ were plotted as a function of W_0, as displayed in **Figure 5**.

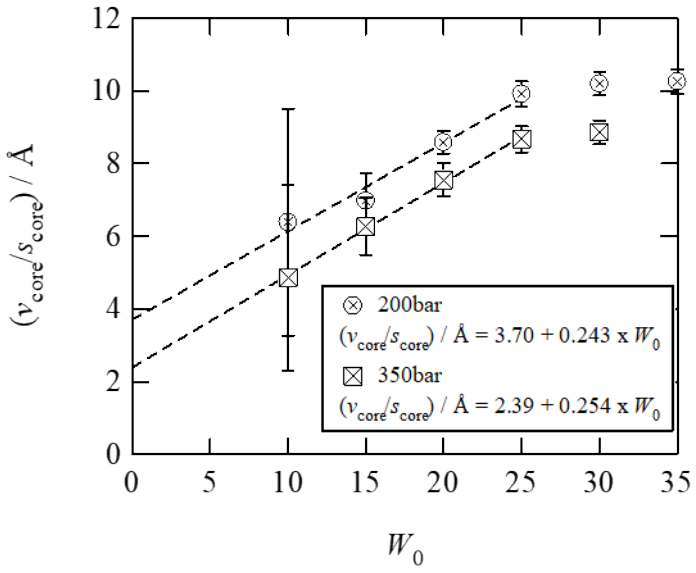

Figure 5. Change in (v_{core}/s_{core}) of prolate cores in 16.7mM $[C_6F_{13}mim][C_6F_{13}S]/D_2O/CO_2$ μEs as a function of W_0 at 45 ºC and 200 bar or 350 bar.

The (v_{core}/s_{core}) data at $W_0 \leq 25$ were expressed as linear functions, suggesting v_{head} and A can be calculated using Equation (2). The values of A, v_{head}, and radius of headgroup ($R_{head} = (3v_{head} / 4\pi)^{1/3}$) obtained from the slopes and the intercepts were (A, v_{head}, R_{head}) = (105 Å^2, 459 Å^3, 4.8 Å) at 200 bar and (101 Å^2, 284 Å^3, 4.1 Å) at 350 bar. At the higher pressures, the headgroup area and volume became smaller, implying a decrease in surfactant cation-anion pair dissociation and/or a decrease in the portion of the head groups immersed in the aqueous cores owing to increased solvation of surfactant tails by CO_2 at the higher pressure (density). Therefore, the increased CO_2 pressure (or density) affects not only tail-CO_2 solvation but also interactions between anionic and cationic headgroups. This could lead to a larger EPP and a lower HCB resulting to the smaller $R_{ell\text{-}a}$ and $R_{ell\text{-}b}$ (i.e. a larger curvature for smaller droplets) at the higher pressures. As compared with anionic double FC-tail surfactants having a sulfonate group, the A and v_{head} values of $[C_6F_{13}mim][C_6F_{13}S]$ at 350 bar are similar to the nFG(EO)$_2$ and nFS(EO)$_2$ (e.g. A and v_{head} were 117-129 Å^2 and 199-231 Å^3 for the fluorinated surfactants in W/CO_2 μEs at 45 ºC and 350 bar, respectively). This is interesting, because of the very different head group structures comparing

these two classes of surfactants. The implication is that the high water solubilization capacities of $[C_6F_{13}mim][C_6F_{13}S]$ in W/CO_2 μEs are linked to the electrostatic ion-pairing, promoting larger EPP and lower HCB values comparable to those of the super-efficient double FC-tail surfactants [7,12,32].

For these $[C_6F_{13}mim][C_6F_{13}S]$ surfactants in scCO_2, the reverse micelle aggregation number (N_{agg}) and occupied area per surfactant molecule at the W/CO_2 microemulsion interface ($A_{C/W}$) were calculated using the following equations.

$$N_{agg} = C_{surf}/C_{micelle} \qquad (3)$$

$$C_{micelle} = (V_{D2O}\, C_{D2O} + V_{head}\, C_{surf})/(V_{core}) = C_{surf}\,(V_{D2O}\, W_0 + v_{head}\, N_A)/(v_{core}\, N_A) \qquad (4)$$

$$A_{C/W} = s_{core}/N_{agg} \qquad (5)$$

where N_A is Avogadro's number, C_{surf} and C_{D2O}, $C_{micelle}$ are molar concentrations of surfactant, D_2O and reverse micelle, v_{core} is volume per D_2O core, V_{D2O}, V_{head}, and V_{core} are molar volumes of D_2O, surfactant headgroups and D_2O cores plus headgroups ($V_{head} = v_{head}\, N_A$, $V_{core} = v_{core}\, N_A$), respectively. For the calculation of $A_{C/W}$ calculation, s_{core} is surface area per D_2O core, being calculated using the ellipsoid radii ($R_{f\text{-}ell,a}$ and $R_{f\text{-}ell,b}$) as well as the calculation of v_{core} for $C_{micelle}$.

According to theory[26-29] the spontaneous packing parameter (SPP) can be obtained by

$$SPP = v_{tail}/(A_0\, l_{tail}) \qquad (6)$$

where v_{tail} and l_{tail} are hydrophobic tail volume and length, respectively. These symbols have the same meanings as in the expression of the EPP.[29] Entropy is taken into account by the fact that the area per molecule minimizes the free energy of the surfactant film (A_0 is the area that minimizes the free energy). According to this approach reverse micelles would be obtained with SPP > 1 (reversed cores form if the surfactant tails orient upward) to ~1 (cylindrical). In the case of W/CO_2 μEs, EPP values should be calculated by taking account of solvation of the head and tail groups with water and CO_2 into the A_0 and v_{tail} values. If the hydrophobic part is assumed to be a truncated cone, the volume should be[13,32]

$$v_{tail} = l_{tail}\{A_{C/W} + A_{tail} + (A_{C/W}\, A_{tail})^{0.5}\}/3 \qquad (7)$$

where A_{tail} is area per hydrophobic tail terminus, respectively. When A_0 is replaced by $A_{C/W}$ for the calculation of EPP in W/CO_2 μEs, Eq. (6) can be simply expressed as

$$\text{EPP} = \{s_{\text{micelle}} + s_{\text{core}} + (s_{\text{micelle}}\, s_{\text{core}})^{0.5}\}/(3s_{\text{core}}) \qquad (8)$$

where s_{micelle} is surface area per reverse micelle. In this study, the values of s_{micelle} were calculated from the ellipsoid core radii ($R_{\text{f-ell,a}}$ and $R_{\text{f-ell,b}}$), with surfactant tail length l_{tail} assumed to be 13.6 Å (between the terminal F-atom and the C-atom bearing the sulfonate group). All the values of $A_{\text{C/W}}$, N_{agg} and EPP obtained by Eqs. (3)-(8) are based on the assumption that all surfactant molecules are adsorbed at the W/CO_2 interface. In actual W/CO_2 μEs, it is likely that some surfactant molecules will partition away from the interface. However, this is estimated to be negligible compared with total number of associated surfactant molecules (8.0 x 10^{-2} mol%), taking into account very low critical microemulsion concentrations in scCO_2 for fluorinated ionic surfactants, which is typically < 10^{-4} mol %.[42] The calculated aggregation properties N_{agg}, $A_{\text{C/W}}$, and EPP for the prolate droplets are listed in **Table S4**. The $A_{\text{C/W}}$ values were 118-134 $Å^2$ at W_0 values of 10-30 and are very close to those of nFG(EO)$_2$ and nFS(EO)$_2$ as mentioned above. [32]

Figure 6 shows changes in N_{agg} and EPP as a function of W_0 for [C_6F_{13}mim][C_6F_{13}S]/D_2O/CO_2 microemulsions at 45 ºC and 200 and 350 bar, using data from **Table S4**. For comparison purposes, the figures also include literature data for double-tail surfactants nFG(EO)$_2$ (n = 4 and 8) in W/CO_2 μEs [32] and the common hydrocarbon surfactant AOT but in W/n-heptane μEs [43].

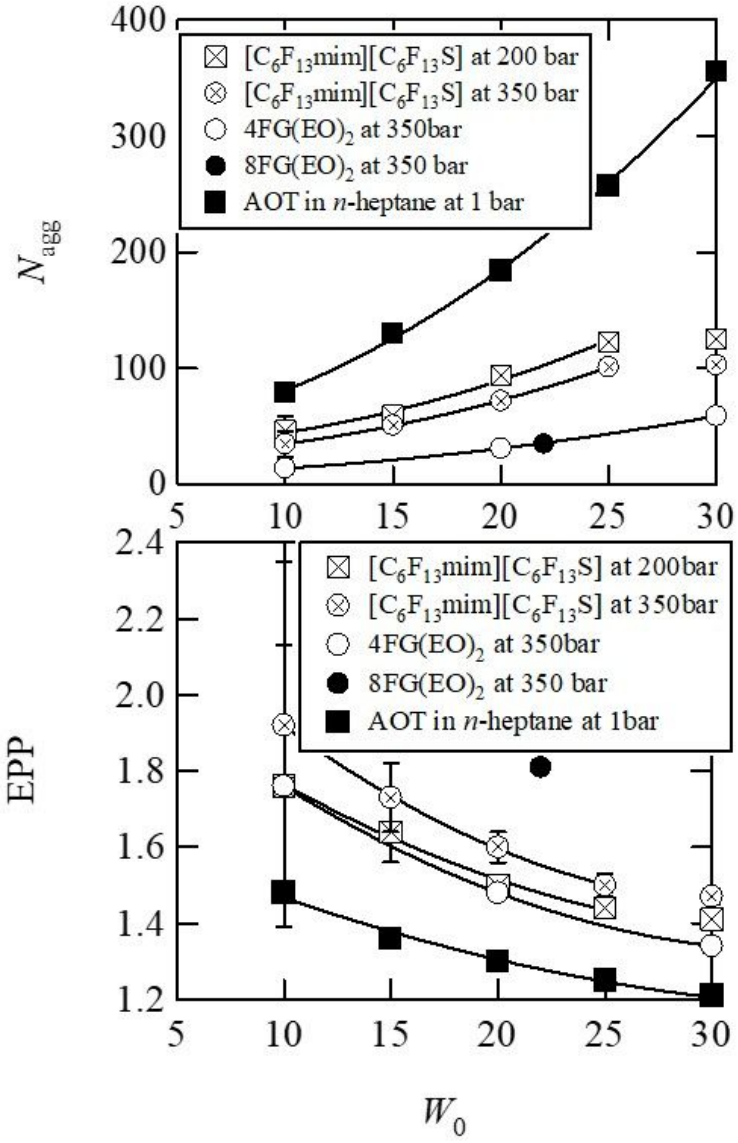

Figure 6. Changes in aggregation number (N_{agg}) and effective packing parameter (EPP) of surfactants as a function of W_0. The data were for D_2O/CO_2 μEs containing 16.7 mM [C_6F_{13}mim][C_6F_{13}S] and 50 mM double FC-tail surfactants (4FG(EO)$_2$ and 8FG(EO)$_2$) at 45 ºC and W/*n*-heptane μEs containing 50 mM AOT at 25 ºC.

As reported for other reverse micellar systems with AOT[43] and the double FC-tail surfactants [32], N_{agg} and EPP for $[C_6F_{13}mim][C_6F_{13}S]$, respectively, increased and decreased with W_0, until the single phase μEs became unstable and turbid phases appeared. This is consistent with an increase in aggregation number for both surfactant and water, as well as a change in surfactant molecular morphology from a reversed truncated cone to a cylindrical shape. These changes are linked to growth of reverse micelles and a decrease in negative curvature of the W/CO_2 interface with increasing water loading. As compared to the double FC-tail anionic $8FG(EO)_2$ and $4FG(EO)_2$ surfactants, the catanionic $[C_6F_{13}mim][C_6F_{13}S]$ generates reverse micelles with larger N_{agg} values than those anionics. This implies that headgroup ion-pairing promotes dense packing of $[C_6F_{13}mim][C_6F_{13}S]$ molecules to favor reverse micelles owing to reduced electrostatic repulsion between headgroups. On the other hand, lowering the pressure from 350 to 200 bar increased N_{agg} and decreased EPP for $[C_6F_{13}mim][C_6F_{13}S]$, presumably due to a promotion of molecular aggregation owing to a reduction in CO_2 solvation of the fluorinated tails at the lower CO_2 density. Comparing the $A_{C/W}$ and v_{head} values for $[C_6F_{13}mim][C_6F_{13}S]$ and the fluorinated double-tail $8FG(EO)_2$ and $4FG(EO)_2$, shows EPP was relatively close to that of $4FG(EO)_2$ but far from the value for $8FG(EO)_2$. Since these two surfactant classes have similar $A_{C/W}$ values, the difference in EPP between them is likely due to the fluorination level of the tails, namely longer FC-tails have the capacity to solvate more CO_2 molecules, giving rise to greater effective tail volumes. As compared with AOT/W/*n*-heptane μEs [43], the W/CO_2 μEs had smaller N_{agg} and larger EPP values. This may be linked to differences in surfactant tail-solvent interactions, in other words, better solvation for the FC-tails with CO_2, as compared to for the AOT-tails with *n*-heptane.

This study demonstrated that the EPP of this catanionic surfactant, comparable to that of anionic double FC-tail surfactants, enables stabilization of W/CO_2 microemulsions with high W_0 values. This is very interesting as ionic headgroups themselves are known to be insoluble in supercritical CO_2 and surfactants having ionic head groups usually require long and/or multiple CO_2-philic tails to stabilize W/CO_2 microemulsions. However, it is now apparent that mixing single CO_2-philic tail anions and cations,

which are alone mostly insoluble and incompatible with CO_2, is a useful approach to design CO_2-philic surfactants.

Conclusions

In order to meet requirements for potential use of W/CO_2 μEs in industrial processes[16-18], W/CO_2 μEs have been studied here, stabilized by ion-pairs of low F-content surfactant anions and cations, which themselves are individually insoluble and surface-inactive in $scCO_2$. Because the ions are strongly associated, they cannot be easily dissociated under ambient conditions, as such, catanionic surfactants are not classified as normal ionic surfactants [25,44,45].

This study was conceived to answer the question "why are ion-paired catanionic surfactants so effective at stabilizing high water content W/CO_2 μEs"? The three new significant findings are:-

(1) The W/CO_2 μEs with $[C_6F_{13}mim][C_6F_{13}S]$ solubilized an ionic dye which acts as a microenvironmental polarity probe, showing behavior similarity to other fluorinated anionic surfactants. [9,12]. On the other hand, the other catanionic surfactants with lower F-content did not solubilize the dye in $scCO_2$, which is consistent with a lack of W/CO_2 μE stabilization.

(2) Aggregation numbers of reverse micelles were about two times larger for $[C_6F_{13}mim][C_6F_{13}S]$ compared with fluorinated double-tail anionic surfactants [32] implying that electrostatic interactions between cationic and anionic headgroups promote close packing of surfactants to stabilize reverse micelles.

(3) Effective packing parameter (EPP) values of the catanionic surfactant in W/CO_2 μEs were relatively close to those found previously for the double perfluorooctyl-tail anionic surfactant $4FG(EO)_2$ [32]. This indicates the electrostatic interactions resulted in a small interfacial areas and volumes for the catanionic headgroups, which is required for reversed curvature self-assembly, as found for the sulfonate headgroup of $4FG(EO)_2$ [32].

From these findings and previous studies [25], the efficiency of $[C_6F_{13}mim][C_6F_{13}S]$ is likely related to EPP and HCB would be consistent with those of double FC-tail anionic surfactants [32]. Such a large EPP and a low HCB would be consistent with the small area and low ionicity of the catanionic headgroup, as compared to the related single-tail and single ionic headgroup anionic and cationic surfactants

($Na[C_6F_{13}S]$ and $[C_6F_{13}mim][CH_3SO_3]$). Hence, the concept of surfactant anion-cation pairing represents a new platform for developing CO_2-philic surfactants and water-in-CO_2 microemulsions for practical applications. This surfactant may be thought of as "the goose (cheap, simple-structure, and CO_2-inactive surfactants) that lays the golden egg (super-efficient CO_2-philic solubilizer)". Using this platform but with highly-methylated alkyl tails, it should be possible to generate cheap and simple hydrocarbon surfactants as a super-efficient CO_2-philic solubilizers, which is a long-cherished dream in supercritical CO_2 science and technology.

ASSOCIATED CONTENT

Supporting Information. Chemical structures of surfactants studied in earlier W/CO_2 microemulsion studies. Calculation of scattering length densities of reverse micelle shells (ρ_{shell}), aqueous cores (ρ_{core}), and CO_2 (ρ_{CO2}) in the D_2O/CO_2 μEs. Pressures at which clear single phases start to appear cloudy, P_{trans} for $[C_6F_{13}mim][C_6F_{13}S]/W/CO_2$ mixtures. UV-vis absorption spectra for aqueous methyl orange (MO) solution/CO_2 mixtures with 16.7 mM $[C_5F_{11}mim][C_5F_{11}S]$ and $[C_6F_{13}mim][(CF_3)_3S]$. Change in absorbance of $[C_6F_{13}mim][C_6F_{13}S]/W/CO_2$ μEs with adding aqueous methyl orange (MO) solution. SANS profiles (Lin-Lin plots) for 16.7mM $[C_6F_{13}mim][C_6F_{13}S]/D_2O/CO_2$ μEs at various W_0 values and pressures. Estimation of D_2O core radii in 16.7 mM $[C_6F_{13}mim][C_6F_{13}S]/D_2O/CO_2$ reverse micelles by Guinier and Porod analyses of SANS data. Estimation of correlation length for 16.7 mM $[C_6F_{13}mim][C_6F_{13}S]/D_2O/CO_2$ microemulsions by Ornstein-Zernicke formalism. Prolate D_2O core radius, aspect ratio, estimated specific viscosity for 16.7 mM $[C_6F_{13}mim][C_6F_{13}S]/D_2O/CO_2$ microemulsions obtained by fitting theoretical curves of prolate ellipsoidal particle model to SANS data. Estimation of reverse micelle concentration, aggregation number, area per surfactant molecule, and effective packing parameter of the D_2O/CO_2 μEs with 16.7 mM $[C_6F_{13}mim][C_6F_{13}S]$ at 45 ºC and 200 bar or 350 bar.

This material is available free of charge via the Internet at "http://pubs.acs.org."

AUTHOR INFORMATION

Corresponding Author. *E-mail sagisaka@hirosaki-u.ac.jp; FAX +81-172-39-3579 (M.S.)

Notes. The authors declare no competing financial interest.

ACKNOWLEDGEMENT

This project was supported by JSPS [KAKENHI, Grant-in-Aid for Scientific Research (B), No. 19H02504, Fostering Joint International Research (A), No. 15KK0221, Grant-in-Aid for Challenging Research (Exploratory), No.17K19002], and Leading Research Organizations (RCUK [through EPSRC EP/I018301/1], ANR [13-G8ME-0003]) under the G8 Research Councils Initiative for Multilateral

Research Funding –G8-2012. We also acknowledge STFC for the allocation of beam time, travel, and consumables grants at ISIS.

References

(1) Beckman, E. J. Supercritical and Near-Critical CO_2 in Green Chemical Synthesis and Processing. *J. Supercrit. Fluids* **2004**, *28*, 121-191.

(2) Goetheer, E. L. V.; Vortaman, M. A. G.; Keurentjes, J. T. F. Opportunities for Process Intensification Using Reverse Micelles in Liquid and Supercritical Carbon Dioxide. *Chem. Eng. Sci.* **1999**, *54*, 1589-1596.

(3) Consani, K. A.; Smith, R. D. Observations on the Solubility of Surfactants and Related Molecules in Carbon Dioxide at 50 ºC. *J. Supercrit. Fluids* **1990**, *3*, 51-65.

(4) Ryoo, W.; Webber, S. E.; Johnston, K. P. Water-in-Carbon Dioxide Microemulsions with Methylated Branched Hydrocarbon Surfactants. *Ind. Eng. Chem. Res.*, **2003**, *42*, 6348-6358.

(5) Lee, H.; Pack, J W.; Wang, W.; Thurecht, K. J.; Howdle, S. M. Synthesis and Phase Behavior of CO_2-Soluble Hydrocarbon Copolymer: Poly(Vinyl Acetate-*alt*-Dibutyl Maleate). *Macromolecules* **2010**, *43*, 2276-2282.

(6) Shi, Q.; Jing, L.; Xiong, C.; Liu, C.; Qiao, W. Solubility of Nonionic Hydrocarbon Surfactants with Different Hydrophobic Tails in Supercritical CO_2. *J. Chem. Eng. Data* **2015**, *60*, 2469–2476.

(7) Sagisaka, M.; Yoda, S.; Takebayashi, Y.; Otake, K.; Kitiyanan, B.; Kondo, Y.; Yoshino, N.; Takebayashi, K.; Sakai, H.; Abe, M. Preparation of a W/scCO_2 Microemulsion Using Fluorinated Surfactants. *Langmuir* **2003**, *19*, 220-225.

(8) Lee, C. T., Jr.; Psathas, P. A.; Johnston, K. P.; deGrazia, J.; Randolph, T. W. Water-in-Carbon Dioxide Emulsions: Formation and Stability. *Langmuir* **1999**, *15*, 6781-6791.

(9) Johnston, K. P.; Harrison, K. L.; Klarke, M. J.; Howdle, S. M.; Heitz, M. P.; Bright, F. V.; Carlier, C.; Randolph, T. W. Water-in-Carbon Dioxide Microemulsions: A New Environment for Hydrophiles Including Proteins. *Science* **1996**, *271*, 624-626.

(10) Zielinski, R. G.; Kline, S. R.; Kaler, E. W.; Rosov, N. A Small-Angle Neutron Scattering Study of Water in Carbon Dioxide Microemulsions. *Langmuir* **1997**, *13*, 3934-3937.

(11) Niemeyer, E. D.; Bright, F. V. The pH within PFPE Reverse Micelles Formed in Supercritical CO_2. *J. Phys. Chem. B* **1998**, *102*, 1474-1478.

(12) Sagisaka, M.; Iwama, S.; Yoshizawa, A.; Mohamed, A.; Cummings S.; Eastoe, J. An Effective and Efficient Surfactant for CO_2 Having Only Short Fluorocarbon Chains. *Langmuir* **2012**, *28*, 10988-10996.

(13) Sagisaka, M.; Ono, S.; James, C.; Yoshizawa, A.; Mohamed, A.; Guittard, F.; Enick, R. M.; Rogers, S. E.; Czajka, A.; Hill, C.; Eastoe, J. Anisotropic Reversed Micelles with Fluorocarbon-Hydrocarbon Hybrid Surfactants in Supercritical CO_2, *Colloids Surf. B* **2018**, *168*, 201-210.

(14) Li, Q.; Li, T.; Wu, J. Water Solubilization Capacity and Conductance Behaviors of AOT and NaDEHP Systems in the Presence of Additives. *Colloids Surf. A* **2002**, *197*, 101-109.

(15) Sagisaka, M.; Hino, M.; Sakai, H.; Abe, M.; Yoshizawa, A. Water/Supercritical CO_2 Microemulsions with a Fluorinated Double-tail Surfactant for Syntheses of Semiconductor Ultrafine Particles. *J. Jpn. Colour Soc. Mater.* **2008**, *81*, 331-340.

(16) Holmes, J. D.; Steytler, D. C.; Rees, G. D.; Robinson B. H. Bioconversions in a Water-in-CO_2 Microemulsion. *Langmuir* **1998**, *14*, 6371–6376.

(17) Van Roosmalen, M. J. E.; Woerlee, G. F.; Witkamp, G. J.; Surfactants for Particulate Soil Removal in Dry-cleaning with High-pressure Carbon Dioxide. *J. Supercrit. Fluids* **2004**, *30*, 97-109.

(18) Luo, D.; Qiu, T.; Lu, Q. Ultrasound-assisted Extraction of Ginsenosides in Supercritical CO_2 Reverse Microemulsions. *J. Sci. Food Agric*. **2007**, *87*, 431-436.

(19) Kravetz, L.; Guin, K. F. Effects of Surfactant Structure on Stability of Enzymes Formulated into Laundry Liquids. *J. Am. Oil Chem. Soc*. **1985**, *62*, 943-949.

(20) Sagisaka, M.; Fujii, T.; Koike, D.; Yoda, S.; Takebayashi, Y.; Furuya, T.; Yoshizawa, A.; Sakai, H.; Abe, M.; Otake, K. Surfactant-Mixing Effects on the Interfacial Tension and the Microemulsion Formation in Water/Supercritical CO_2 System. *Langmuir* **2007**, *23*, 2369-2375.

(21) Sagisaka, M.; Koike, D.; Mashimo, Y.; Yoda, S.; Takebayashi, Y.; Furuya, T.; Yoshizawa, A.; Sakai, H.; Abe, M.; Otake, K. Water/supercritical CO_2 Microemulsions with Mixed Surfactant Systems. *Langmuir* **2008**, *24*, 10116–10122.

(22) Huang, J.-B.; Zhao, G. -X. Formation and Coexistence of the Micelles and Vesicles in Mixed Solution of Cationic and Anionic Surfactant. *Colloid Polym. Sci.* **1995**, *273*, 156–164.

(23) Upadhyaya, A.; Acosta, E. J.; Scamehorn, J. F.; Sabatini, D. A. Microemulsion Phase Behavior of Anionic-Cationic Surfactant Mixtures: Effect of Tail Branching. *J. Surfactants Deterg.* **2006**, *9*, 169-179.

(24) Eastoe, J.; Dalton, J.; Rogueda, P.; Sharpe, D.; Dong, J.; Webster, J. R. P. Interfacial Properties of a Catanionic Surfactant. *Langmuir* **1996**, *12*, 2706-2711.

(25) Sagisaka, M.; Saito, T.; Yoshizawa, A.; Rogers, S. E.; Guittard, F.; Hill, C.; Eastoe, J.; Blesic, M. Water-in-CO_2 Microemulsions Stabilized by Fluorinated Cation–Anion Surfactant Pairs. *Langmuir* **2019**, *35*, 3445–3454.

(26) Pleines, M.; Kunz, W.; Zemb, T. Understanding and Prediction of the Clouding Phenomenon by Spontaneous and Effective Packing Concepts. *J. Surfact. Deterg.* **2019**, *22*, 1011–1021.

(27) Ontiveros, J. F.; Pierlot, C.; Catté, M.; Molinier, V.; Pizzino, A.; Salager, J.-L.; Aubry, J.-M. Classification of ester oils according to their Equivalent Alkane Carbon Number (EACN) and asymmetry of fish diagrams of $C_{10}E_4$/ester oil/water systems. *J. Colloid Interf. Sci.* **2013**, *403*, 67–76.

(28) Israelachvili, J. N. Measurements of Hydration Forces Between Macroscopic Surfaces. *Chem. Scr.* **1985**, *25*, 7-14.

(29) Nagarajan, R. Molecular Packing Parameter and Surfactant Self-Assembly: The Neglected Role of the Surfactant Tail. *Langmuir* **2002**, *18*, 31–38.

(30) Span, R.; Wagner, W. A New Equation of State for Carbon Dioxide Covering the Fluid Region from the Triple-Point Temperature to 1100 K at Pressures up to 800 MPa. *J. Phys. Chem. Ref. Data* **1996**, *25*, 1509-1596.

(31) Kotlarchyk, M.; Chen, S.-H.; Huang, J. S.; Kim, M. W. Structure of Three-Component. Microemulsions in the Critical Region Determined by Small Angle Neutron Scattering Data. *Phys. Rev. A* **1984**, *29*, 2054-2069.

(32) Sagisaka, M.; Iwama, S.; Ono, S.; Yoshizawa, A.; Mohamed, A.; Cummings, S.; Yan, C.; James, C.; Rogers, S. E.; Heenan, R. K.; Eastoe, J. Nanostructures in Water-in-CO_2 Microemulsions Stabilized by Double-chain Fluorocarbon Solubilizers. *Langmuir* **2013**, *29*, 7618−7628.

(33) Guinuier, A.; Fournet, G. *Small-Angle Scattering of X-Rays*, Wiley, New York, 1956.

(34) Karukstis, K. K.; Savin, D. A.; Loftus, C.T.; D'Angelo, N. D. Spectroscopic Studies of the Interaction of Methyl Orange with Cationic Alkyltrimethylammonium Bromide Surfactants. *J. Colloid Interf. Sci.* **1998**, 203, 157–163.

(35) Kline, S. R. Reduction and Analysis of SANS and USANS Data Using IGOR Pro. *J. Appl. Cryst.* **2006**, *39*, 895–900.

(36) Almásy, L.; Turmine, M.; Perera, A. Structure of Aqueous Solutions of Ionic Liquid 1-Butyl-3-methylimidazolium Tetrafluoroborate by Small-Angle Neutron Scattering. *J. Phys. Chem. B* **2008**, 112, 2382- 2387.

(37) Zemb, T. N.; Klossek, M.; Lopian, T.; Marcus, J.; Schöettl, S.; Horinek, D.; Prevost, S. F.; Touraud, D.; Diat, O.; Marčelja, S.; Kunz, W. How to Explain Microemulsions Formed by Solvent Mixtures without Conventional Surfactants. *Proc. Natl. Acad. Sci.* **2016**, *113*, 4260–4265.

(38) Grimaldi, N.; Rojas, P. E.; Stehle, S.; Cordoba, A.; Schweins, R.; Sala, S.; Luelsdorf, S.; Piña, D.; Veciana, J.; Faraudo, J.; Triolo, A.; Braeuer, A. S.; Ventosa, N. Pressure-Responsive, Surfactant-Free CO_2-Based Nanostructured Fluids. *ACS Nano* **2017**, *11*, 10774–10784.

(39) Weber, A.; Stühn, B. Structure and Phase Behavior of Polymer Loaded Non-ionic and Anionic Microemulsions. *J. Chem. Phys.* **2016,** *144*, 144903.

(40) Williams, D. F. Extraction with Supercritical Gases. *Chem. Eng. Sci*. **1981**, *36*, 1769-1788.

(41) Orr, F. M.; Taber, J. J. Use of Carbon Dioxide in Enhanced Oil Recovery. *Science* **1984**, *224*, 563-569.

(42) Sagisaka, M.; Fujii, T.; Ozaki, Y.; Yoda, S.; Takebayashi, Y.; Kondo, Y.; Yoshino, N.; Sakai, H.; Abe, M.; Otake, K. Interfacial Properties of Branch-Tailed Fluorinated Surfactants Yielding a Water/Supercritical CO_2 Microemulsion. *Langmuir* **2004**, *20*, 2560-2566.

(43) Nave, S.; Eastoe, J.; Heenan, R.K.; Steytler, D.; Grillo, I. What is so Special about Aerosol-OT? 2. Microemulsion Systems. *Langmuir* **2000**, *16*, 8741-8748.

(44) Yin, H.; Lin, Y.; Huang, J.; Ye, J. Temperature-Induced Vesicle Aggregation in Catanionic Surfactant Systems: The Effects of the Headgroup and Counterion. *Langmuir* **2007**, *23*, 4225–4230.

(45) Nakama, Y.; Harusawa, F.; Murotani, I. Cloud Point Phenomena in Mixtures of Anionic and Cationic Surfactants in Aqueous Solution. *J. Surfactants Deterg.* **1990**, *67*, 717-721.

TOC (Revised)

Sagisaka, M. et al.